Advanced optical interference filters based on metal and dielectric layers

Thomas Begou, Fabien Lemarchand, Julien Lumeau

Advanced optical interference filters based on metal and dielectric layers

THOMAS BEGOU, FABIEN LEMARCHAND, AND JULIEN LUMEAU*

Aix Marseille Univ, CNRS, Centrale Marseille, Institut Fresnel, Marseille, France
**julien.lumeau@fresnel.fr*

Abstract: In this paper, we investigate the design and the fabrication of an advanced optical interference filter based on metal and dielectric layers. This filter respects the specifications of the 2016 OIC manufacturing problem contest. We study and present all the challenges and solutions that allowed achieving a low deviation between the fabricated prototype and the target.

OCIS codes: (310.1620) Interference coatings; (310.1860) Deposition and fabrication; (310.3915) Metallic, opaque, and absorbing coatings; (310.4165) Multilayer design.

References and links

1. A. V. Tikhonravov, M. K. Trubetskov, and G. W. DeBell, "Optical coating design approaches based on the needle optimization technique," Appl. Opt. **46**, 704-710 (2007).
2. A. V. Tikhonravov and M. K. Trubetskov, "Modern design tools and a new paradigm in optical coating design," Appl. Opt. **51**, 7319-7332 (2012).
3. M. Trubetskov, T. Amotchkina, and A. Tikhonravov, "Automated construction of monochromatic monitoring strategies," Appl. Opt. **54**, 1900-1909 (2015).
4. H. Ehlers, D. Ristau, "Advanced control and modeling of deposition processes," Chinese Optics Letters **s1**(11), S10203 (2013).
5. A. Zöller; M. Boos; H. Hagedorn; B. Romanov, "Computer simulation of coating processes with monochromatic monitoring," Proc. SPIE **7101**, Advances in Optical Thin Films III, 71010G (25 September 2008).
6. K. D. Hendrix; C. A. Hulse; G. J. Ockenfuss; R. B. Sargent, "Demonstration of narrowband notch and multi-notch filters," Proc. SPIE **7067**, Advances in Thin-Film Coatings for Optical Applications V, 706702 (29 August 2008).
7. M. Scherer, J. Pistner, and W. Lehnert, "UV- and VIS filter coatings by plasma assisted reactive magnetron sputtering (PARMS)," in Optical Interference Coatings, OSA Technical Digest (Optical Society of America, 2010), paper MA7.
8. T. Begou, H. Krol, D. Stojcevski, F. Lemarchand, M. Lequime, C. Grezes-Besset, J. Lumeau, "Complex optical interference filter with stress compensation," Proc. SPIE **9627**, Optical Systems Design 2015: Advances in Optical Thin Films V, 96270R (September 23, 2015).
9. T. Amotchkina, M. K. Trubetskov, Y. Pervak, L. Veisz, and V. Pervak, "Stress compensation with antireflection coatings for ultrafast laser applications: from theory to practice," Opt. Express **22**, 30387-30393 (2014).
10. Optics Balzers, "Design and manufacturing of spectral filters with low large angle scatter," ESA project Summary report, LLAS-RP-OBJ-1030, Issue A2, 21/11/2014.
11. H. Qi, M. Zhu, M. Fang, S. Shao, C. Wei, K. Yi and J. Shao, "Development of high-power laser coatings," High Power Laser Science and Engineering **1**(1), pp 36 – 43 (2013).
12. K. Olson, A. Ogloza, J. Thomas and J. Talghader, "High power laser heating of low absorption materials," J. Appl. Phys. **116**, 123106 (2014).
13. L. Frey, P. Parrein, L. Virot, C. Pellé, and J. Raby, "Thin film characterization for modeling and optimization of silver-dielectric color filters," Appl. Opt. **53**, 1663-1673 (2014).
14. Shumei Yang, "Circular, variable, broad-bandpass filters with induced transmission at 200–1100 nm," Appl. Opt. **32**, 4836-4842 (1993).
15. M. Khardani, M. Bouaïcha, and B. Bessaïs, "Bruggeman effective medium approach for modelling optical properties of porous silicon: comparison with experiment," Phys. Status Solidi C **4**: 1986–1990.
16. J.A. Dobrowolski, S. Browning, M. Jacobson and M. Nadal, "Topical meeting on Optical Interference Coatings (OIC' 2001): manufacturing problem," Appl. Opt. **41**, 3039-3052 (2002).
17. J.A. Dobrowolski, S. Browning, M. Jacobson and M. Nadal, "2004 Optical Society of America's topical meeting on Optical Interference Coatings: manufacturing problem," Appl. Opt. **45**, 1303-1311 (2006).
18. J.A. Dobrowolski, Li Li, M. Jacobson and D.W. Allen, "2010 topical meeting on Optical Interference Coatings: manufacturing problem," Appl. Opt. **50**, C408-C419 (2011).

19. L. Li, J. A. Dobrowolski, M. Jacobson, and C. Cooksey, "Broadband transmission filters from the 2013 Optical Interference Coatings manufacturing problem contest," Appl. Opt. **53**, A248-A258 (2014).
20. J.A. Dobrowolski, S. Browning, M. Jacobson and M. Nadal, "2007 topical meeting on Optical Interference Coatings: manufacturing problem," Appl. Opt. **47**, C231-C245 (2008).
21. http://www.osa.org/en-us/meetings/topical_meetings/optical_interference_coatings/oic_current_topic_problem_contests/
22. D. Poitras, L. Li, M. R. Jacobson, and C. Cooksey, "OIC 2016 manufacturing problem contest," in Optical Interference Coatings 2016, OSA Technical Digest (online) (Optical Society of America, 2016), paper WC.1.
23. F Lemarchand, "Application of clustering global optimization to thin film design problems," Opt. Express **22**, 5166-5176 (2014).
24. J. A. Dobrowolski, "Completely automatic synthesis of optical thin film systems," Appl. Opt. **4**, 937-946 (1965).
25. P. B. Johnson and R. W. Christy, "Optical constants of transition metals: Ti, V, Cr, Mn, Fe, Co, Ni, and Pd," Phys. Rev. B **9**, 5056-5070 (1974).
26. A. Zoeller, M. Boos, H. Hagedorn, W. Klug, and C. Schmitt, "High accurate in-situ optical thickness monitoring," in Optical Interference Coatings, OSA Technical Digest Series (Optical Society of America, 2004), paper TuE10.
27. R. R. Willey, "Simulation comparisons of monitoring strategies in narrow bandpass filters and antireflection coatings," Appl. Opt. **53**, A27-A34 (2014).

1. Introduction

Optical filters that use the interference effect to obtain spectral transmission and reflection are very classical optical elements that are used in a wide variety of optical systems, e.g. in telecommunication, biophotonics, industry, buildings. These optical functions are obtained by combining thin layers with different refractive indices and thickness onto a substrate. They allow achieving an almost infinite number of spectral functions including bandpass filters (narrowband and broadband filters), edge filters (longpass and shortpass filters), notch filters (from single to multiple), beamsplitters (polarized or not), mirror coatings… There have been tremendous progresses over the past 15-20 years in the field of thin film filters. First of all, with the increase of computational capabilities associated with the development of more and more sophisticated design procedures and algorithms [1,2], it is now possible to find solutions to most of physical design problem using commercial software. However, one must always keep in mind that these designed multilayer stacks must also be in accordance with the fabrication capabilities. For example, it is well-known that the fabrication of homogeneous ultra-thin layers is very challenging. Therefore algorithms in conventional software generally investigate whether it is possible or not to remove these layers without affecting too much the performances of the filter. Another limitation is related to the precision that can be achieved for the control of the thickness of each layer, and this precision is highly dependent on the used monitoring technique. In order to predict and perfectly adapt the monitoring strategy with the stack design, there have been large efforts toward the development of so-called "Virtual Deposition Process" (VDP), i.e. software that enable to simulate a deposition, and therefore take into account all the fluctuations, errors, processing methods… in order to predict the performances of a filter after fabrication without running the experiment [3-5]. While these VDPs have some limitations as it is hard to perfectly reproduce the exact experimental conditions within software, they have proven to be of prime interest as they provide a new way for the development of optimal monitoring strategies.

In addition to these theoretical developments, and thanks to the development of process automation, there also have been astonishing developments in the deposition and monitoring techniques. It is now possible to run full-automated depositions lasting several tens of hours and containing several hundreds of layers and with total stack thickness of several tens of microns [6]. While electron beam deposition is one of the most conventional techniques for the fabrication of optical interference filters, sputtering has proven to be a better choice for a large number of applications as it provides more stable and repeatable deposition rates. Among the various sputtering techniques that are available, plasma assisted reactive

magnetron sputtering combined with a stable a repeatable optical monitoring system, has proven to be a very reliable technique when it comes to complex multilayer filters [7]. Various examples of complex filters, especially for space applications, where requirement are very strict, can be found in the literature [8-10].

For most of the applications that were just mentioned before, the spectral requirements are either on the transmission or on the reflection properties of the filters and in most of the cases, the sum of the transmission and of the reflection of the filter is equal to one. These optical functions are achieved by using stacks only composed with dielectric layers. Thus, large efforts have been placed on minimizing the absorption and scattering losses in these filters. Actually, many developments have been carried out towards the decrease of absorption losses, especially for high energy and high power lasers [11] and other efforts have been made in order to minimize scattering losses that can bring very large parasitic light especially in imaging systems for space or astronomy applications [10,12]. By the combination of two dielectric materials, it is then possible to design and fabricate most of lossless optical functions. There are however cases where the use of dielectric layers is not optimal or does not allow achieving the required performances. For example, the design and the fabrication of some broadband elements such as mirrors require the deposition of a large number of layers. But depending on the application and the required specifications, they can be easily replaced by a single metallic layer (or a combination of one metallic layer and a few dielectric layers for protected or enhanced mirrors). Another example is when the optical function to be fabricated should have losses, i.e. when the sum of the transmission and the reflection is not equal to one. In this case, it is required to include metallic (or absorbing) layers, thin enough to still secure a non-zero transmission (when required). Such an approach was used for the fabrication of color filters [13] or induced bandpass filters [14]. However, including such layers is very challenging as they are generally very thin and very sensitive to thickness errors. Also, they generally interact with the surrounding layers, especially if those one are oxide layers, resulting in the appearance of transition zones with partially oxidized metallic layer and eventually a mixture between the metallic and the dielectric species [15].

In this paper, we investigated the design and the manufacturing of advanced optical interference filters based on metal and dielectric layers. Over the past twenty years, the organizers of the Optical Interference Coating Conference (OIC) of the Optical Society of America have been proposing several contests opened to the whole thin film community. These contests aimed in testing the state-of-the-art in multilayer thin film design, fabrication and measurement. Among those one, the manufacturing problem contest is the one that requires the broadest expertise as it requires designing, manufacturing and characterizing a very specific component. Every time, the spectral target transmission and reflection was not related to a specific application but more to a specific design and fabrication problem. The first one aimed in showing how to produce irregularities [16], the second one how to produce elements at oblique incidence [17], the fourth aimed in showing how to produce an element with several orders of magnitude differences in transmittance [18], and the fifth problem was to produce a filter with regular shape and sharp transitions over an extended spectral region [19]. All the previously cited problems required the deposition of a large number of layers but did not require any metallic or absorbing layers. Only the third manufacturing contest required combining dielectric and metallic layers. The goal of this contest was to produce a filter with reflected and transmitted beams meeting specific colorimetric coordinates and this did not require designing and fabricating filter with more than ~20 layers. [20]. The 2016 OIC manufacturing contest aimed in fabricating a filter which spectral dependence of the transmission (T) and the reflection (R) between 400 and 1100 nm produce a moose head [21,22]. Due to the complex and broad spectrum response, the design of such function requires several tens of layers with various thicknesses. The number of layers will depend on the expected merit function defined as the mean error over as the sum of the transmission and

the reflection. Also, due to the fact that R ≠ 1 – T, the design requires including one or several metallic layers. This manufacturing problem appeared as an ideal example in order to study and tackle some of the problems that have been previously described as well as to provide one possible solution for each of them. In this paper, we first present a strategy for the design of such spectral filters and then present an experimental demonstration including the various strategies that were implemented to achieve a filter with a low merit function.

2. Filter design

The theoretical targets, that produce the drawing of a moose head, are defined in both reflectance and transmittance within [400-1100] nm spectral range with a 2.5 nm interval [21,22]. The lower part (in solid red line) of the head corresponds to the transmittance target and the upper part (in dotted red line) to the reflectance target (see Figure 1).

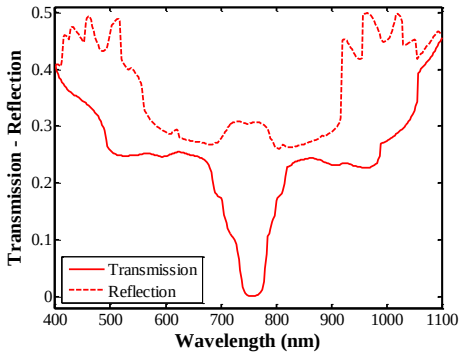

Fig. 1. Theoretical spectral targets of a Moose head. In solid line – Transmittance and in dotted line – Reflectance at 7° angle of incidence.

In order to define the deviation between the target and the spectral performances of the designed structures, we defined a merit function (MF):

$$MF = \frac{1}{2N}\left[\sum_{i=1}^{N}\left(T_i - T_{exp,i}\right)^2 + \left(R_i - R_{exp,i}\right)^2\right]^{1/2}. \quad (1)$$

where T_i and $T_{exp,i}$ are respectively the targeted and measured transmittance values (at normal incidence), R_i and $R_{exp,i}$ are respectively the targeted and measured reflectance values (near normal incidence, i.e. at 7° for un-polarized light) at the specified wavelength λ_i and N is the total number of wavelengths. Note that both transmittance and reflectance are expressed in percent (note that the values displayed in all spectra were multiplied by 100 to calculate the MF).

Let us first analyze the difficulties associated with the design of such a structure. First of all, finding a design fitting both transmittance and reflectance is challenging: reflectance and transmittance are totally uncorrelated with an absorbance varying from 10% to 70% depending on the wavelength. The use of at least three materials, two transparent and one metallic is thus mandatory. An approximation of the total Optical Thickness (OT) for a design corresponding to the transmitted and reflectance targets can be obtained by a simple visual analysis of both targets. Whereas transmittance spectra does not show high frequency spectral fringes, the reflectance curve exhibits high frequency oscillations in [420-520] nm and [920-1030] nm regions, corresponding to the moose head antler upper part. The pseudo-periodic frequency of oscillations is within 30 nm in the 950 nm region. Achieving similar frequency oscillations at 950 nm with a single layer requires an OT of ~12 µm. One can then expect a similar OT for a corresponding Moose head design. To confirm this rough estimation, let us first consider the partial problem consisting in finding a solution for only the reflectance target. In this case, the problematic is far easier as a pair of two transparent dielectric

materials is enough to reproduce this target. We considered Nb_2O_5 and SiO_2 as respectively high and low refractive index materials, with an index of refraction about $n(Nb_2O_5) = 2.28$ and $n(SiO_2) = 1.47$ @ 800 nm (i.e. the one obtained using PARMS deposition technique). For a non-absorbing problem, needle optimization with a single high index layer as starting design gives good results. Table 1 presents, for a given starting OT, the number of layers of the final design using needle optimization, its final OT and the corresponding MF. An OT of about 10 µm and about 90 layers are necessary to obtain a MF lower than 1.0. A similar approach considering now only the transmittance target is described on Table 2. In this case, a MF lower than 1.0 is obtained for designs with only 7 µm OT and about 60 layers.

Design #	OT starting design (µm)	Number of layers	OT final design (µm)	MF
D1-1	4	42	4.16	1.44
D1-2	5	51	5.19	1.39
D1-3	6	59	5.67	1.37
D1-4	7	62	6.89	1.33
D1-5	8	72	8.34	1.21
D1-6	9	92	9.87	0.93
D1-7	10	92	10.31	0.9
D1-8	11	93	10.75	0.88
D1-8	12	101	12.05	0.82

Table 1. Designs associated with a single reflectance target.

Table 2. Designs associated with a single transmittance target.

Design #	OT starting design (µm)	Number of layers	OT final design (µm)	MF
D2-1	4	41	4.33	1.33
D2-2	5	56	5.49	1.03
D2-3	6	55	5.79	1.02
D2-4	7	63	6.97	0.79
D2-5	8	77	8.10	0.60
D2-6	9	79	9.22	0.49
D2-7	10	89	9.55	0.47
D2-8	11	85	10.42	0.45
D2-8	12	94	11.88	0.39

For the Moose head total design problem, the total OT seems then to be essentially imposed by reflectance target. The introduction of a thin metallic layer will help to match the absorbance, but will not help to reduce the OT. One can then expect to find a satisfying design solution with an OT between 10 and 12 µm and a number of layers around 90. As there is no obvious starting design, the first strategy consisted in using the needle design technique with a single thick dielectric layer. In this case, this quasi universal method did not give good results with a final MF higher than 4.0 whatever be the initial thickness of the layer. Our approach then consisted in using a global optimization procedure [23] with several random 40-layer starting designs composed with alternated Nb_2O_5 and SiO_2 layers and one layer of chromium. Then the most promising optimized 40-layer solutions were improved by

increasing OT and the number of layers by a gradual evolution procedure [24]. The choice of chromium as metal does not seem critical, and similar results can be obtained with other low reflective metallic materials. We used the chromium refractive index given by ref [25]. Table 3 presents 8 different solutions for this problem with an increasing OT from 8 up to 15 µm. One can see that increasing the OT of the final design, allows decreasing the MF from 1.59 down to 0.91. We then analyzed into more details the Design #D3-7 as it combines a good MF with a number of layers equal to the one of Design #D3-5.

Table 3. Designs associated with both reflectance and transmittance targets.

OT design (µm)	OT design (µm)	Number of layers	MF
D3-1	8.26	68	1.44
D3-2	8.66	75	1.39
D3-3	9.702	89	1.37
D3-4	10.14	95	1.33
D3-5	10.66	105	1.21
D3-6	10.98	115	0.93
D3-7	13.30	105	0.9
D3-8	14.76	121	0.88

Figure 2 shows the refractive index profile of the design #D3-7. In design #D3-7, 5 layers present a thickness between 5 and 10 nm and 26 layers have a physical thickness lower than 20 nm. Layer 67 is a 7.1 nm thick chromium layer. The MF of 0.97 is the minimum achievable with this design, however it is important to stress that this value cannot be experimentally reached since a 0.1 nm thickness variation or a small variation of 0.05 regarding the real part or imaginary part of chromium refractive index will increase the MF to a value higher than 1.0. Moreover, the insertion of several chromium layers was then tested. The improvement of the MF value was shown to be very marginal. Moreover, whatever the number of layers, the total thickness of chromium layers seems constant. This result is not suitable for practical aspects as it would require including layers with thicknesses lower than 4 nm.

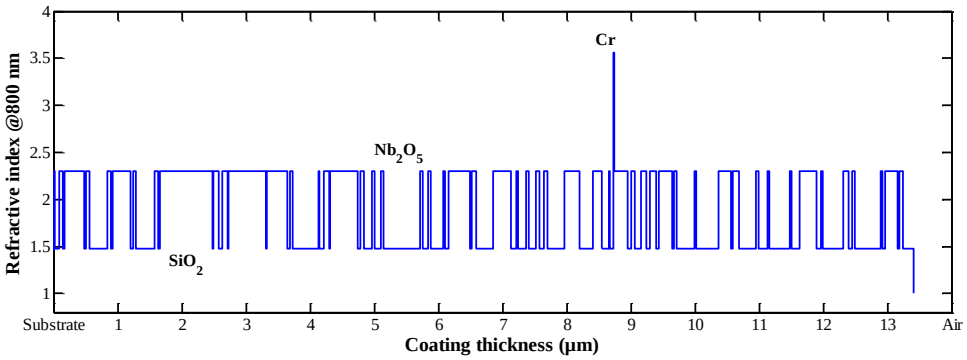

Fig. 2. Profile of the real part of the refractive index (vs. thickness) for the design #D3-7.

Finally, we tested the stability of the design #D3-7. We calculated the increase of the MF when an absolute error of +0.2 nm is performed on a single layer and for each layer while keeping all other thickness equal to the designed one (Figure 3). For more than 25 layers, in particular the metallic layer and high index layers above it, a 0.2 nm uncompensated single error leads to an increase of more than 0.1 of the MF value. This result shows that this design

is very sensitive to manufacturing errors and that the monitoring strategy will play a key role in the final performances of the fabricated filter.

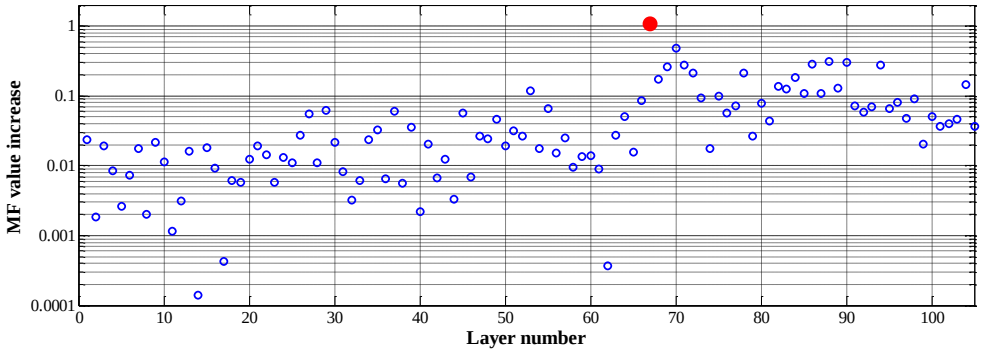

Fig. 3. MF value sensitivity on a small thickness variation (+0.2 nm) of a single layers of design #D3-7 and for each layer while keeping all other thickness equal to the designed one. Red point identifies the metallic layer.

3. Filter fabrication

The designed structure that was selected is the D3-7. It is composed with 105 layers made out of Nb_2O_5 and SiO_2, except for the layer #67 made out of chromium. These layers have various thicknesses ranging from a few nanometers up to a few hundred of nanometers. The design does not show specific periodicity and is therefore very challenging to fabricate. In addition, the insertion of a thin metallic layer within the multilayer stack further increases the complexity of the fabrication. In order to overcome all these difficulties, we opted for Plasma Assisted Reactive Magnetron Sputtering (PARMS) and used a Bühler HELIOS machine to perform these depositions [7]. This machine, combined with an Optical Monitoring System (Bühler OMS 5000) allows precisely controlling the thickness of each layer with a precision within a few 0.1% for each layer [26]. This system allows in-situ monitoring at a single wavelength of the transmission of a thin film filter during its fabrication and integrates turning point and trigger point monitoring strategies [27].

However, achieving such high precision on the thickness of each of the layers requires defining an optimal monitoring strategy. Actually, we used trigger point (TP) strategy combined with percent of optical extrema monitoring (POEM) [27]. While TP strategy uses precalculated transmission level at a given wavelength to stop the deposition of each layer, POEM uses the same strategy but partially corrects manufacturing errors by recalculating, during the deposition, the next TP based on the error between the previous theoretical and experimental extremum. To define the optimal strategy, we used a commercial simulation software from Bühler (*mcalc)* in order to identify the optimal monitoring wavelengths and ran an associated Virtual Deposition Process (VDP) software, also provided by Bühler, in order to test whether the determined strategy is valid or not. In order to separate the problems (i.e. complex dielectric stack and metallic layer), we decided to split the coating into three distinct parts:

- **Part 1**: Dielectric stack from layer 1 to 66
- **Part 2**: Metal layer 67
- **Part 3**: Dielectric stack from layer 68 to 105

Let us now analyze each of these different parts.

Part 1 is composed with alternated Nb_2O_5 and SiO_2 dielectric layers. We first decided to look for an optimal strategy that allows monitoring the whole stack using a single test glass. Due to the widely varying thicknesses, it is not possible to use a single monitoring

wavelength as it would be classically done with a Fabry-Perot cavity [27]. The strategy was optimized with POEM strategy, using the conditions that the trigger point must be different from the next turning point by a quantity larger than 5% and also that the trigger point is more than 5% or less than 95% of the peak-to-valley amplitude of the measured signal. It uses 9 different wavelengths (from 450 to 800 nm) and, based on the monitoring criteria, we could not find an optimal solution that uses a lower number of wavelengths. Using this monitoring strategy, we ran a minimum of 10 VDP simulations in order to validate it. We supposed two types of contribution to the optical monitoring noise: a multiplicative noise equal to $0.030 \pm 0.005\%$ and an additive noise equal to $0.004 \pm 0.005\%$, whose exact amplitude is spectrally dependent and is applied on a normalized simulated monitoring signal. Noise factors were randomly calculated from a Gaussian distribution. After running a few simulations, we found that the strategy is always diverging, and therefore, it is not possible to monitor these layers with a single test glass. This can be explained by the fact that the designed structure is very sensitive to fabrication errors, especially for the metallic layers and the high refractive index layers after it (see Figure 3). In addition, every time the monitoring wavelength is changed, the strategy becomes more and more sensitive to the errors on the previous layers and, the partial error compensation which is classically assumed with POEM, is suddenly severely affected with a new monitoring wavelength. This results in an increasingly unstable strategy that fails after a few changes of the monitoring wavelength. To overcome this problem, we opted for a strategy using different test glasses, each one monitored with a different wavelength. Using this approach, only 5 different monitoring wavelengths are required (Table 4). VDP simulations were run again and showed that such a strategy allows minimizing the errors on the thickness of each of the layers and therefore secures a final spectral shape with errors on the transmission not exceeding a few percent. Each monitoring strategy for each test glasses was run 10 times on VDP simulation software giving an average simulated transmission with standard deviation. MF for each test glass was calculated from these simulations with an uncertainty of 3σ.

Table 4. Monitoring strategy of the Part 1 of the multilayer design.

Test glass number	Layers number	Monitoring wavelength
T1-1	1-12	950 nm
T1-2	13-24	750 nm
T1-3	25-34	490 nm
T1-4	35-50	476 nm
T1-5	51-66	700 nm

We applied the defined strategy for the manufacturing of the Part 1 of the designed structure. For each of the test glass, we measured the spectral dependence of the experimental transmission between 400 and 1100 nm and performed a comparison between the theoretical MF (calculated from the VDP simulations) and the experimental MF (calculated from the measured spectra after deposition) for each test glass and the substrate that was coated with the whole stack (Table 5). We can see that the simulated and experimental MF are well matched for each test glass as well as for the whole Part 1 confirming the usefulness of the VDP simulations in the definition of the optical monitoring procedure. In addition, one can also note that the RMS value (equal to 2.67) of the MF of the complete filter is quite large, showing that the designed structure is very sensitive to manufacturing errors. Such large RMS value can be easily justified by the fact that while trying to properly define the oscillations of the moose head antler upper part, small errors on some of the layers can result in anti-phase oscillations and a large increase of the MF.

Table 5. Average error between theory and experiment for each of the different test glass and for the substrate coated with the whole Part 1.

Test glass number	Layers number	Simulated MF	Experimental MF
T1-1	1-12	0.17 ± 1.40	0.25
T1-2	13-24	0.18 ± 1.60	0.85
T1-3	25-34	0.42 ± 1.07	1.38
T1-4	35-50	0.16 ± 0.69	0.63
T1-5	51-66	0.12 ± 0.81	0.92
Complete	1-66	0.70 ± 2.67	2.58

Figure 4 presents the transmission curves for the test glass #T1-1 (smallest deviation) and #T1-3 (largest deviation) and Figure 5 the transmission of glass substrate coated with the whole Part 1. We can see that these spectra possess a good agreement between theory and experiment associated with a MF of 2.58. From these measurements we could perform reverse engineering on each test glass and confirm that the errors carried out on the thickness of each layer are not higher than a few percent in worse cases.

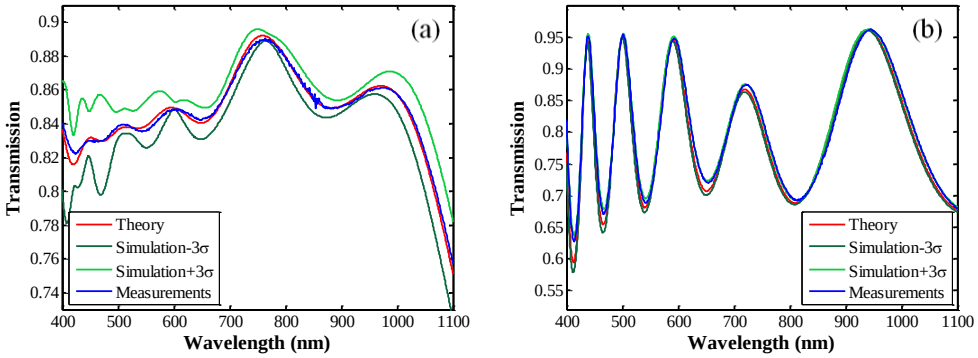

Fig. 4. Spectral dependence of the transmission of the test glass #T1-1 (left, a) and #T1-3 (right, b) of Part 1. In blue the theory and in red the experimental one.

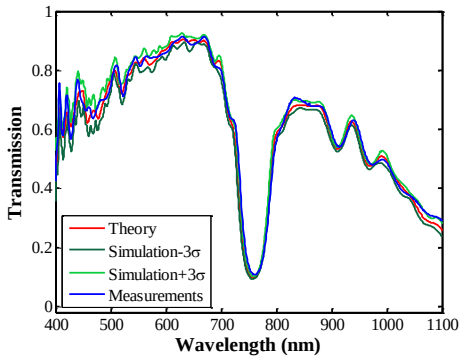

Fig. 5. Spectral dependence of the transmission of the glass substrate coated with the whole Part 1. In blue the theory and in red the experimental one.

Part 2 of the design is composed with a metallic layer. In order to calibrate this part of the stack and account for the problems associated with the partial oxidation of the metallic layer, the error on the refractive index dispersion of the metallic layer and the error on the metallic thickness (that could not be easily monitored using the OMS 5000), we first studied the properties of a 5-layer stack composed with the layers 65 to 69. This intermediate stack consisted thus in depositing two dielectric layers, then the thin metallic layer, and finally two dielectric layers directly onto an uncoated substrate. Spectral measurements were done between 400 and 1100 nm.

Then, we used the following strategy:

- First we determined the metallic thickness by fitting both transmission and reflection spectra. We supposed that the thickness and the refractive index dispersion of the dielectric layers are equal to the designed one and we performed an optimization on the thickness of the chromium layer using tabulated refractive index dispersion [25].
- Then, using this obtained value of physical thickness of the chromium layer, we determined for each wavelength λ_0 the values of the real part and imaginary parts of the refractive index of the chromium layer. The best fit between experimental and modeled $R(\lambda_0)$ and $T(\lambda_0)$ gave new $n(\lambda_0)$ and $k(\lambda_0)$ curves that were finally smoothed.

Figure 6 shows the experimental and modeled transmission and reflection curves obtained after performing the whole process on the 5-layer stack. One can see that with this method, we can obtain an excellent agreement between theoretical and experimental curves.

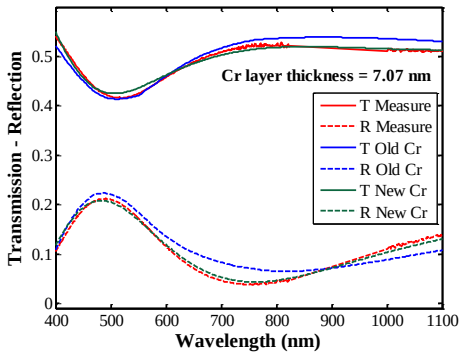

Fig. 6. Spectral dependence of the transmission (solid line) and the reflection (dashed line) of the glass substrate coated with the layers 65 to 69. In red experimental data, in blue theoretical data with chromium index from [24] and in green theoretical data with new chromium index.

A thickness value of 7.07 nm was extracted for the chromium layer. In addition, we compare in Table 6 the values of the extracted real part n and imaginary part k of the refractive index of the chromium layer with the one of the literature for a few distinct wavelengths [25].

Table 6. Comparison between the values of the extracted real part ($n(\lambda_0)$) and imaginary part ($k(\lambda_0)$) of the refractive index of the chromium layer and the one of the literature for a few distinct wavelengths [25]

Wavelength	$n(\lambda_0)_{exp}$	$k(\lambda_0)_{exp}$	$n(\lambda_0)_{litt}$	$k(\lambda_0)_{litt}$
397 nm	1.90	2.83	2.00	2.83
496 nm	2.76	3.30	2.75	3.30
582 nm	3.20	3.30	3.22	3.30
704 nm	3.57	3.27	3.05	3.39

900 nm	3.89	3.22	3.30	3.52
1088 nm	4.05	3.20	3.58	3.58

While this approach is simple to implement, it can have some limitations as the thickness of the chromium layers is determined using inaccurate refractive dispersions, i.e. the one from literature. However, it is important to stress that the second step of our procedure is not a complete determination of the refractive index dispersion of the chromium layer but more a refinement of the Johnson's one as only small, but important for our goal, variations were extracted. In addition, the excellent agreement between the experimental and theoretical transmission and reflection curves tends to prove that the extracted value of the thickness is close to the real one. But, if there is an error, this error is most probably compensated by the optimization that was performed on the refractive index dispersion curves.

As it was shown in Figure 3, the chromium layer is the most critical layer for the whole design and an error of 0.2 nm on its thickness is even too large to allow achieving a final filter having small deviation from the target transmission and reflection. Precision within 0.1 nm or better is thus required. To overcome this problem, we performed the deposition of the Part 2 of the design, i.e. the metallic layer, directly, on top of the sample that was already coated with the Part 1 and reoptimized the design of Part 3, in order to take into account the new opto-geometrical parameters of the chromium layer.

Part 3 is the last of the design and composed with 38 dielectric layers. We used a similar strategy than the one applied for the deposition of the Part 1, i.e. the use of multiple test glasses for optical monitoring. Table 7, gives the monitoring strategy, with their respective MF, that was defined for the Part 3.

Table 7. Monitoring strategy of the Part 3 of the multilayer design.

Test glass number	Layers number	Monitoring wavelength
T3-1	68-73	515 nm
T3-2	74-87	465 nm
T3-3	88-105	690 nm

For this part, we used 3 test glasses associated with 3 different monitoring wavelengths. For each of the test glass, we measured the spectral dependence of the experimental transmission between 400 and 1100 nm and computed the mean deviation between theory and experiment for each test glass and the substrate that was coated with the whole stack (Table 8).

Table 8. Average error between theory and experiment for each of the different test glass and for the substrate coated with the whole Part 3.

Test glass number	Layers number	Simulated MF	Experimental MF
T3-1	68-73	0.12 ± 0.27	0.48
T3-2	74-87	0.13 ± 0.36	1.32
T3-3	88-105	0.23 ± 1.14	0.80
Complete	68-105	0.50 ± 1.45	2.24

Figure 7 presents the transmission curves for the test glass #T3-1 (smallest deviation) and #T3-2 (largest deviation) and Figure 8 the transmission of glass substrate coated with the whole Part 3. We can see that these spectra possess a good agreement between theory and experiment associated with a MF of 2.24.

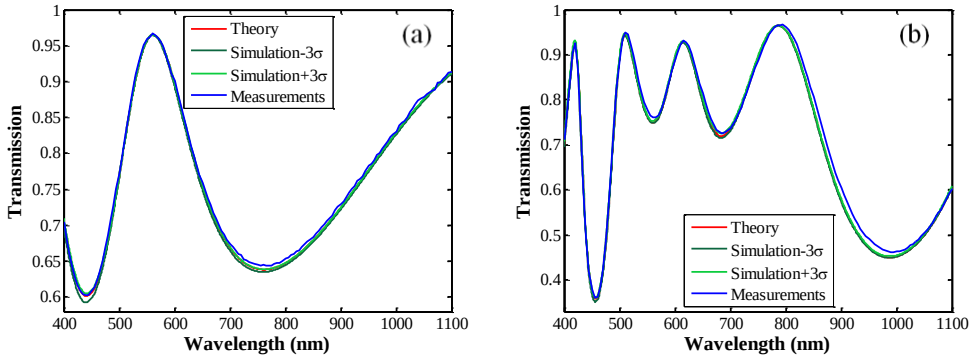

Fig. 7. Spectral dependence of the transmission of the test glass #T3-1 (left, a) and #T3-2 (right, b) of Part 3. In blue the theory and in red the experimental one.

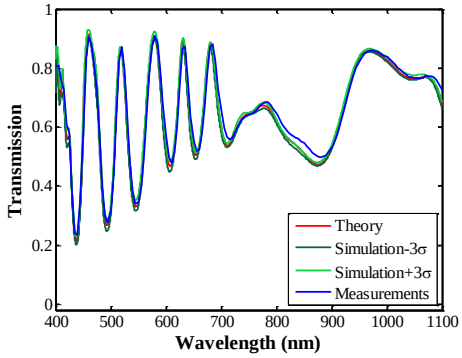

Fig. 8. Spectral dependence of the transmission of the glass substrate coated with the whole Part 3. In blue the theory and in red the experimental one.

Finally, Figure 9 shows the spectral dependence of the transmission and the reflection of the whole 105-layer stack between 400 and 1100 nm and compares this result with the target transmission and reflection spectral profiles. In order to evaluate the result, we calculated for the experimental curve the MF within the whole spectral range. A MF of 2.5 is achieved which is less than three times the theoretical value and confirms that, despite the error sensitivity of the design, minimal errors have been achieved.

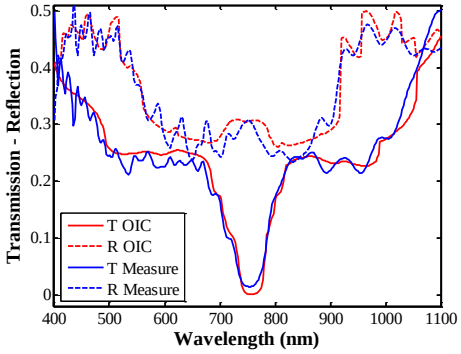

Fig. 9. Spectral dependence of the transmission and the reflection of the glass substrate coated with the whole stack defining the moose head. In red the OIC target and in blue the experimental curve.

4. Conclusion

A complete description of the design and the fabrication procedures of an advanced optical interference filter based on metal and dielectric layers was presented. We first analyzed the difficulties in designing such a component using conventional design tools due to the presence of absorption and showed that using the combination of global optimization procedure with needle technique, it is possible to obtain a promising, but complex and error-sensitive, design composed with 105 layers and a single metallic layer. We then fabricated such a filter using plasma-assisted reactive magnetron sputtering. Using virtual deposition process, we first validated the monitoring procedure. It is based on the decomposition of the design into three different parts, i.e. the dielectric layers between the substrate and the metallic layer, the metallic layer, and the remaining dielectric layers. Optical monitoring of the dielectric layers was carried out using respectively 5 and 3 different test glasses for the first part and the third part of the design. We also developed a specific procedure to account for the specific properties of the metallic layer. Using the combination of all these strategies, we managed to demonstrate an optical filter with complex shape and a good merit function within 2.5.